ACS Catalysis

pubs.acs.org/acscatalysis

Research Article

Enhancing the Chemo-Enzymatic One-Pot Oxidation of Cyclohexane via In Situ H_2O_2 Production over Supported Pd-Based Catalysts

Joseph Brehm,[⊥] Richard J. Lewis,*[,⊥] Thomas Richards, Tian Qin, David J. Morgan, Thomas E. Davies, Liwei Chen, Xi Liu,* and Graham J. Hutchings*

Cite This: *ACS Catal.* 2022, 12, 11776−11789

Read Online

ACCESS | Metrics & More | Article Recommendations | Supporting Information

ABSTRACT: The combination of an evolved unspecific peroxygenase (UPO), from *Agrocybe aegerita* (PaDa-I variant) and bimetallic Pd-based catalysts, is demonstrated to be highly effective for the one-pot oxidative valorization of cyclohexane to cyclohexanol and cyclohexanone (collectively KA oil), via the in situ formation of H_2O_2 from the elements. The alloying of Pd with Zn in particular is found to significantly enhance catalytic performance compared to bimetallic PdAu or monometallic Pd analogues. The improved activity of the $PdZn/TiO_2$/PaDa-I system is attributed to the facile formation of PdZn alloys and the resulting electronic modification of Pd, which results in an inhibition of competitive chemo-catalyzed H_2O_2 degradation reactions and the total suppression of the overoxidation of cyclohexanol. By comparison, the large population of Pd-only clusters present in both the PdAu and monometallic Pd catalysts is considered to be responsible for the promotion of further oxidation products and the unselective conversion of H_2O_2 to H_2O, which hampers overall process efficiency. Notably, given the susceptibility of the enzyme to deactivation at moderate H_2O_2 concentrations, the continual supply of low levels of the oxidant via in situ production represents a highly attractive alternative to the continuous addition of preformed H_2O_2 or co-enzyme-based systems.

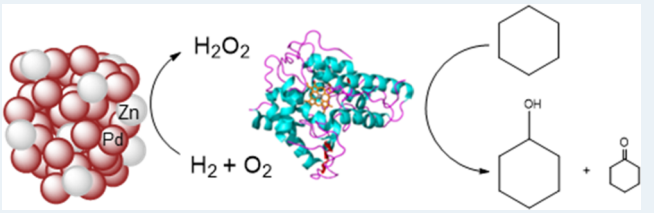

KEYWORDS: *palladium−zinc, hydrogen peroxide, peroxygenase, oxidation, cascade*

INTRODUCTION

Selective oxidation of cyclohexane to KA oil (cyclohexanol and cyclohexanone) is a key industrial process in the manufacture of caprolactam and adipic acid, which are in turn utilized in the production of Nylon-6 and Nylon-6,6. The conventional route to KA oil via an aerobic oxidative process typically utilizes relatively high reaction temperatures (140−180 °C) and homogeneous transition-metal catalysts,[1−3] with rates of substrate conversion typically limited to ∼5% to inhibit overoxidation of the desired products. Indeed, even at moderate rates of conversion, a substantial concentration of ring-opened byproducts, such as 6-hydroxyhexanoic and glucaric acids, may be produced.[4]

The high energy costs associated with the use of elevated reaction temperatures and the added complexity related to the separation of homogeneous species from product streams have led to increasing interest in the use of heterogeneous alternatives to aerobic cyclohexane oxidation. The replacement of molecular oxygen with alternative oxidants including *tert*-butylhydroperoxide (TBHP)[5] and H_2O_2 (either preformed[6,7] or generated in situ[8,9]) has been shown to allow for the utilization of significantly reduced reaction temperatures. However, particularly in the case of the in situ oxidative approach, rates of conversion are still much lower than those of the aerobic route, which is itself deliberately limited.

Alternatively, enzymatic approaches are highly attractive for selective C−H bond activation.[10] In particular, unspecific peroxygenases (UPOs), which are heme-thiolate enzymes of fungal origin, are able to utilize H_2O_2 for the functionalization of C−H bonds with high stereo- and chemoselectivities.[11,12] While UPOs do not rely on sacrificial redox co-factors and auxiliary flavoproteins, which have limited the utilization of alternative heme-containing enzymes, such as P450 monooxygenases, their application on an industrial scale has been somewhat limited by their high sensitivity toward H_2O_2 concentrations.[13] A range of approaches have been developed to supply H_2O_2 to UPOs, including the use of enzymatic cascades, such as those based around glucose oxidase (GOx), formate oxidase (FOx), or choline oxidase (ChOx).[14−17] However, the generation of H_2O_2 via enzymatic cascades has so far been hampered by poor atom efficiency and the production of undesirable side products, such as gluconic acid in the case of the GOx system. While concerns associated with byproduct formation have been overcome through the

Received: June 25, 2022
Revised: September 1, 2022

development of the FOx/UPO route, there is a need to continually maintain reaction solution pH via acid titration, which may limit adoption on an industrial scale.[18] Alternatively, the supply of H_2O_2 via photocatalytic systems has been described, with these approaches limited by a combination of enzyme deactivation through exposure to UV radiation and reactive oxygen species including $^{\bullet}OH$ and $^{\bullet}O_2^-$, in addition to the elevated costs related to the upscaling of photocatalytic transformations.[19]

Recently, we have reported the coupling of in situ H_2O_2 generation, over immobilized PdAu nanoparticles, which are well known to offer high activity toward H_2O_2,[20] with the laboratory-evolved UPO from *Agrocybe aegerita*, referred to as PaDa-I, to achieve selective C−H bond activation.[21] Indeed, there are many efficiency benefits of an in situ approach, including the avoidance of side product formation, which typically results from co-enzyme-based systems or the dilution of product streams, which can result from the use of preformed H_2O_2. However, similarly to the direct synthesis of H_2O_2, there is clearly a concern associated with the direct mixing of gaseous mixtures of H_2 and O_2 and the use of reagent mixtures outside of the explosive regime and ideally below the lower flammability limit would be preferable, particularly for application at scale.

For the chemo-catalytic/enzymatic cascade approach to rival the current approach to C−H bond activation, further advances with respect to the inhibition of chemo-catalyzed competitive reactions are necessary, in particular given the need for highly pure product streams and the ability of active metals to also promote H_2O_2 degradation pathways, which in turn limits selective H_2 utilization. With this in mind, we now investigate a range of Pd-based chemo-catalysts, focusing on nonprecious secondary metals to improve economic viability, for the selective oxidation of cyclohexane to KA oil, when used in conjunction with PaDa-I.

EXPERIMENTAL SECTION

Mono- and bi-metallic 1%Pd-X/TiO_2 catalysts (where Pd/X = 1:1 (wt/wt) and X = Au, Pt, Fe, Ni, Zn, In, Co, and Cu) have been prepared via an excess chloride co-impregnation procedure, based on a methodology previously reported in the literature,[22] which has been shown to improve dispersion of metal species, particularly Au. In all cases, chloride-based metal precursors have been utilized, with the requisite amount of metal precursors used for the synthesis of the mono- and bi-metallic catalysts reported in Table S1. The procedure to produce 0.5%Pd−0.5%Au/TiO_2 (2 g) is outlined below, with a similar methodology utilized for all catalysts.

Aqueous acidified $PdCl_2$ solution (1.667 mL, 0.58 M HCl, [Pd] = 6 mg mL^{-1}, Merck) and aqueous $HAuCl_4{\cdot}3H_2O$ solution (0.8263 mL, [Au] = 12.25 mg mL^{-1}, Strem Chemicals) were mixed in a 50 mL round-bottom flask and heated to 65 °C with stirring (1000 rpm) in a thermostatically controlled oil bath, with total volume fixed to 16 mL using H_2O (HPLC grade, Fischer Scientific). Upon reaching 65 °C, TiO_2 (1.98 g, Degussa, P25) was added over the course of 5 min with constant stirring. The resulting slurry was stirred at 65 °C for a further 15 min, following this the temperature was raised to 95 °C for 16 h to allow for complete evaporation of water. The resulting solid was ground prior to a reductive heat treatment (5% H_2/Ar, 400 °C, 4 h, 10 °C min^{-1}).

Surface area measurements of key catalytic materials, as determined by five-point N_2 adsorption are reported in Table S2. The corresponding analysis by X-ray diffraction is reported in Figure S1A,B, with no reflections associated with immobilized metals observed, which may be indicative of the high dispersion of metal species.

Unspecific Peroxygenase Preparation. Evolved AaeUPO (PaDa-I variant) designed in Saccharomyces cerevisiae was overproduced in Pichia pastoris in a bioreactor and purified to homogeneity (Reinheitszahl value [*Rz*] [A_{418}/A_{280}] ∼2.4). Enzyme activities were determined using ABTS as substrate. Reactions were done in triplicate. 20 μL PaDa-I was added to 180 μL ABTS reaction mixture (100 mM sodium citrate−phosphate pH 4.4 with 0.3 mM ABTS and 2 mM H_2O_2) and substrate conversion was followed by measuring the absorption at 418 nm (ε_{418} = 36 000 M^{-1} cm^{-1}). The PaDa-I concentration was appropriately diluted to give rise to linear enzyme kinetics. One unit is defined as the amount of enzyme that converts 1 μmol of substrate in 1 min.

Catalyst Testing. Note 1: in all cases, reactions were run multiple times, over multiple batches of catalyst, with the data being presented as an average of these experiments. Catalytic activity was found to be consistent to within ±3% on the basis of multiple reactions.

Note 2: reaction conditions used within this study operate outside the flammability limits of gaseous mixtures of H_2 and O_2.[23]

Note 3: the conditions used within this work for H_2O_2 synthesis and degradation using high-pressure batch conditions have previously been investigated, with the presence of CO_2 as a diluent for reactant gases and a methanol co-solvent in the case of the high-pressure experiments identified as key to maintaining high catalytic efficacy toward H_2O_2 production.[22]

Direct Synthesis of H_2O_2 from H_2 and O_2, Under High-Pressure Batch Conditions. Hydrogen peroxide synthesis was evaluated using a Parr Instruments stainless steel autoclave with a nominal volume of 100 mL, equipped with a PTFE liner and a maximum working pressure of 2000 psi. To test each catalyst for H_2O_2 synthesis, the autoclave liner was charged with catalyst (0.01 g) and HPLC-grade solvents (5.6 g of methanol and 2.9 g of H_2O, both Fischer Scientific). The charged autoclave was then purged three times with 5%H_2/CO_2 (100 psi) before filling with 5%H_2/CO_2 to a pressure of 420 psi, followed by the addition of 25%O_2/CO_2 (160 psi). Pressures of 5%H_2/CO_2 and 25%O_2/CO_2 are given as gauge pressures and reactant gasses were not continually supplied. The reaction was conducted at a temperature of 2 °C, for 0.5 h with stirring (1200 rpm), with the reactor temperature controlled using a HAAKE K50 bath/circulator using an appropriate coolant.

H_2O_2 productivity and H_2O_2 concentrations (wt %) were determined by titrating aliquots of the final solution after reaction with acidified $Ce(SO_4)_2$ (0.0085 M) in the presence of a ferroin indicator. Catalyst productivities are reported as $mol_{H_2O_2}$ kg_{cat}^{-1} h^{-1}.

Total autoclave capacity was determined via water displacement to allow for accurate determination of H_2 conversion and H_2O_2 selectivity. When equipped with a PTFE liner, the total volume of an unfilled autoclave was determined to be 93 mL, which includes all available gaseous space within the autoclave.

Catalytic conversion of H_2 and selectivity toward H_2O_2 were determined using a Varian 3800 GC fitted with TCD and equipped with a Porapak Q column.

https://doi.org/10.1021/acscatal.2c03051
ACS Catal. 2022, 12, 11776−11789

H_2 conversion (eq 1) and H_2O_2 selectivity (eq 2) are defined as follows

$$H_2 \text{ conversion } (\%) = \frac{\text{mmol}_{H_2\,(t(0))} - \text{mmol}_{H_2\,(t(1))}}{\text{mmol}_{H_2\,(t(0))}} \times 100 \quad (1)$$

$$H_2O_2 \text{ selectivity } (\%) = \frac{H_2O_2 \text{ detected (mmol)}}{H_2 \text{ consumed (mmol)}} \times 100 \quad (2)$$

Degradation of H_2O_2, Under High-Pressure Batch Conditions. Catalytic activity toward H_2O_2 degradation (via hydrogenation and decomposition pathways) was determined in a similar manner to that used to measure the direct synthesis activity of a catalyst. The autoclave liner was charged with methanol (5.6 g, HPLC standard, Fischer Scientific), H_2O_2 (50 wt %, 0.69 g, Merck), H_2O (2.21 g, HPLC standard, Fischer Scientific), and catalyst (0.01 g), with the solvent composition equivalent to a 4 wt % H_2O_2 solution. From the solution, prior to the addition of the catalyst, two 0.05 g aliquots were removed and titrated with acidified $Ce(SO_4)_2$ solution using ferroin as an indicator to determine an accurate concentration of H_2O_2 at the start of the reaction. The autoclave was purged three times with 5%H_2/CO_2 (100 psi) before filling with 5% H_2/CO_2 to a gauge pressure of 420 psi. The reaction was conducted at a temperature of 2 °C, for 0.5 h with stirring (1200 rpm). After the reaction was complete, the catalyst was removed from the reaction mixture by filtration and two 0.05 g aliquots were titrated against the acidified $Ce(SO_4)_2$ solution using ferroin as an indicator. The degradation activity is reported as $\text{mol}_{H_2O_2}\ \text{kg}_{cat}^{-1}\ \text{h}^{-1}$.

Direct Synthesis of H_2O_2 from H_2 and O_2, Under Low-Pressure Batch Conditions. Reactions were carried out in 50 mL gas-tight round-bottom flasks rated to 60 psi and stirred using a Radleys 6 Plus Carousel equipped with a gas distribution system. The catalyst (0.001 g) was weighed directly into the glass flasks. To this was added potassium phosphate buffer (10 mL, 100 mM, pH 6.0) prepared with KH_2PO_4 and K_2HPO_4 (both obtained from Merck). Subsequently, the flask was sealed, purged, and pressurized to 29 psi with H_2 (23 psi) and air (6 psi) to give a reaction atmosphere containing 80% H_2 and 20% air. The reaction mixtures were stirred (250 rpm) at ambient temperature (20 °C) for 2 h, unless otherwise stated. After the desired reaction time, the vessel was depressurized and the H_2O_2 concentration was determined by UV−vis spectroscopy. To determine H_2O_2 concentration an aliquot (1.5 mL) of the post-reaction solution was combined with potassium titanium oxalate dihydrate solution acidified with 30% H_2SO_4 (0.02 M, 1.5 mL) resulting in the formation of an orange pertitanic acid complex. This resulting solution was analyzed spectrophotometrically using an Agilent Cary 60 UV−vis spectrophotometer at 400 nm by comparison to a calibration curve by taking aliquots of H_2O_2 in the buffer solution (1.5 mL) and adding acidified potassium titanium oxalate dihydrate solution (1.5 mL).

Degradation of H_2O_2, Under Low-Pressure Batch Conditions. Catalytic activity toward H_2O_2 degradation (via hydrogenation and decomposition pathways) was determined in a similar manner to that used to measure the direct synthesis activity of a catalyst, under low-pressure conditions. The potassium phosphate buffer (10 mL, 100 mM, pH 6.0) prepared with KH_2PO_4 and K_2HPO_4 (both obtained from Merck) and H_2O_2 (2000 ppm, Merck) were added into the 50 mL gas-tight round-bottom flask. From the solution, prior to the addition of the catalyst, two 0.05 g aliquots were removed to allow for the quantification of the initial H_2O_2 concentration via UV−vis spectroscopy. Subsequently, the catalyst (0.001 g) was added to the flask, which was then sealed, purged, and pressurized to 29 psi with H_2 (23 psi) and N_2 (6 psi) to give a reaction atmosphere containing 80% H_2 and 20% N_2. The reaction mixtures were stirred (250 rpm) at ambient temperature (20 °C) for 2 h. After the desired reaction time, the vessel was depressurized, the catalyst was removed via filtration, and the remaining H_2O_2 was quantified by UV−vis spectroscopy.

Metal Leaching Studies. To provide an indication of the extent of metal leaching during the in situ cyclohexane oxidation reaction, indicative model studies were conducted in the absence of the enzyme and substrate (i.e., under low-pressure H_2O_2 direct synthesis conditions) utilizing 0.01 g of the heterogeneous catalyst (i.e., 10 times that utilized for the cyclohexane oxidation reaction), with all other conditions as outlined as above.

Catalytic Testing of the Tandem Chemo-Bio System for Cyclohexane Oxidation. The role of the chemo-catalyst/enzyme ratio has previously been identified to be crucial in optimizing the overall efficiency of a number of processes.[24,25] Given the susceptibility of the enzyme to deactivate in the presence of even mild concentrations of H_2O_2 and the role of the chemo-catalyst in promoting competitive H_2O_2 degradation pathways, it is clear that optimizing this parameter is crucial for achieving maximum process efficiency. As such, and with a focus on key catalyst formulations, a series of cyclohexane oxidation experiments were conducted using a fixed mass of chemo-catalyst (0.001 g) and varied concentration of enzyme (15−45 U mL_{RM}^{-1}) (Figure S2 and associated supplementary note), with an optimal PaDa-I concentration of 15 U mL_{RM}^{-1} identified.

Reactions were carried out in a 50 mL gas-tight round-bottom flask rated to 60 psi and stirred using a Radleys 6 Plus Carousel equipped with a gas distribution system. Typically, the reaction mixtures contained 15 U mL_{RM}^{-1} PaDa-I (23 μL), 0.1 mg mL_{RM}^{-1} of the metal catalyst (0.001 g) in potassium phosphate buffer (10 mL, 100 mM, pH 6) and cyclohexane (10 mM). The catalysts were weighed directly into the glass vessels followed by the additon of the buffer solution. Immediately before starting the reactions, the enzyme and substrate were added. The sealed reaction vessels were pressurized to 29 psi with H_2 (23 psi) and air (6 psi) to give a reaction atmosphere containing 80% H_2 and 20% air. The reactions were stirred with a magnetic stirrer bar at 250 rpm at ambient temperature (20 °C) for 2 h unless otherwise stated. After the desired reaction time, product formation was monitored by extracting with 2 × 5 mL ethyl acetate containing 1-decanol (2 mM) as the internal standard and subjecting aliquots of the organic layer to GC analysis (Agilent model 7658 equipped with a CP Wax 52 CB column). Additionally, residual H_2O_2 concentration was determined by UV−vis spectroscopic analysis of the aqueous layer, as outlined above.

Cyclohexane conversion (eq 3) and product (cyclohexanol or cyclohexanone) selectivity (eq 4) were determined as follows

https://doi.org/10.1021/acscatal.2c03051
ACS Catal. 2022, 12, 11776−11789

$$\text{cyclohexane conversion (\%)} = \frac{\text{mmol}_{\text{cyclo }(t(0))} - \text{mmol}_{\text{cyclo }(t(1))}}{\text{mmol}_{\text{cyclo }(t(0))}} \times 100 \quad (3)$$

$$\text{product selectivity (\%)} = \frac{\text{mmol}_{\text{product }(t(1))}}{\text{mmol}_{\text{cyclo }(t(0))} - \text{mmol}_{\text{cyclo }(t(1))}} \times 100 \quad (4)$$

Further in situ oxidation studies were carried out to determine the efficacy of using, preformed H_2O_2 at levels identical to those achieved if all of the H_2 in the system was converted to H_2O_2 and also identical to net H_2O_2 concentrations achieved over a 2 h direct synthesis study (50 ppm), under identical conditions. Notably, for these low concentration studies, we have investigated both commercially supplied H_2O_2 (Merck) (i.e., in the presence of stabilizers) and that generated in our autoclave system (i.e., in the absence of stabilizers and utilizing the aqueous buffered solution used for the enzymatic reactions). Additional studies were conducted under individual gaseous reagents (H_2 and O_2 as air). In the case of those experiments conducted using commercial H_2O_2total reaction pressure was fixed to 29 psi using N_2. For experiments using either H_2 or air alone, total pressure was also maintained at 29 psi using N_2 in addition to the reagent gas.

Additional cyclohexanol oxidation studies were conducted in the presence of the PaDa-I enzyme, and homogeneous metals at a concentration comparable to that leached from the heterogeneous catalyst during a standard tandem reaction (i.e., using 0.001 g of catalyst), as informed by our model leaching studies. Such studies were conducted under an inert atmosphere (N_2, 29 psi) in the presence of preformed H_2O_2 (50 ppm, Merck) for 2 h, with all other conditions as outlined above.

Note 4: operating the in situ cyclohexane and cyclohexanol oxidation reactions using a reaction solution pH of 6 was considered to represent a compromise between H_2O_2 and enzyme stability.[26]

Evaluating Efficacy toward the Oxidation of Cyclohexanol. The separate efficacy of the PaDa-I enzyme or the heterogeneous catalysts toward the oxidation of cyclohexanol was determined in a similar manner to that used to determine the activity of the chemo-enzymatic system toward cyclohexane oxidation, as outlined above.

The reaction mixtures contained 15 U mL_{RM}^{-1} PaDa-I (23 μL) or 0.1 mg mL_{RM}^{-1} of the metal catalyst (0.001 g) in potassium phosphate buffer (10 mL, 100 mM, pH 6) and cyclohexanol (10 mM). When using the heterogeneous catalyst, the materials were weighed out directly into the glass vessels followed by the buffer solution and substrate. The sealed reaction vessels were pressurized to 29 psi with H_2 (23 psi) and air (6 psi) to give a reaction atmosphere containing 80% H_2 and 20% air. The reactions were stirred (250 rpm) at ambient temperature (20 °C) for 2 h. After the desired reaction time, product formation was monitored by extracting with 2 × 5 mL ethyl acetate containing 1-decanol (2 mM) as the internal standard and subjecting aliquots of the organic layer to GC analysis (Agilent model 7658 equipped with a CP Wax 52 CB column).

A similar procedure to that outlined above was utilized when investigating the efficacy of the enzyme alone. However, in addition to the phosphate buffer and substrate, preformed H_2O_2 (Merck) was also added, at a concentration comparable to that generated by the heterogeneous catalysts over a 2 h in situ reaction (50 ppm). The sealed reaction vessels were pressurized to 29 psi with N_2 prior to stirring with a magnetic stirrer bar at 250 rpm at ambient temperature (20 °C) for 2 h. After the desired reaction time, product formation was monitored by extracting with 2 × 5 mL ethyl acetate containing 1-decanol (2 mM) as the internal standard and subjecting aliquots of the organic layer to GC analysis (Agilent model 7658 equipped with a CP Wax 52 CB column).

Catalyst Characterization. The bulk structure of the catalysts was determined by powder X-ray diffraction using a (θ–θ) PANalytical X'Pert Pro powder diffractometer using a Cu Kα radiation source, operating at 40 keV and 40 mA. Standard analysis was carried out using a 40 min run with a back-filled sample, between 2θ values of 10–80°. Phase identification was carried out using the International Centre for Diffraction Data (ICDD).

Brunauer–Emmett–Teller (BET) surface area measurements were conducted using a Quadrasorb surface area analyzer. A five-point isotherm of each material was measured using N_2 as the adsorbate gas. Samples were degassed at 250 °C for 2 h prior to the surface area being determined by five-point N_2 adsorption at −196 °C, and data were analyzed using the BET method.

A Thermo Scientific K-Alpha$^+$ photoelectron spectrometer was used to collect XP spectra utilizing a micro-focused monochromatic Al Kα X-ray source operating at 72 W. Data were collected over an elliptical area of ∼400 μm^2 at pass energies of 40 and 150 eV for high-resolution and survey spectra, respectively. Sample charging effects were minimized through a combination of low-energy electrons and Ar^+ ions; consequently, this resulted in a C (1s) line at 284.8 eV for all samples. All data were processed using CasaXPS v2.3.24 using a Shirley background, Scofield sensitivity factors,[27] and an electron energy dependence of −0.6 as recommended by the manufacturer.

DRIFTS measurements were taken on a Bruker Tensor 27 spectrometer fitted with a mercury cadmium telluride (MCT) detector. A sample was loaded into the Praying Mantis high temperature (HVC-DRP-4) in situ cell before exposure to N_2 and then 1% CO/N_2 at a flow rate of 50 cm^3 min^{-1}. A background spectrum was obtained using KBr, and measurements were recorded every 1 min at room temperature. Once the CO adsorption bands in the DRIFT spectra ceased to increase in size, the gas feed was changed back to N_2 and measurements were repeated until no change in subsequent spectra was observed.

Aberration-corrected scanning transmission electron microscopy (AC-STEM) was performed using a probe-corrected Hitachi HF5000 S/TEM, operating at 200 kV. The instrument was equipped with bright field (BF) and annular dark-field (ADF) detectors for high-spatial-resolution STEM imaging experiments. This microscope was also equipped with a secondary electron detector and dual Oxford Instruments XEDS detectors (2 × 100 mm^2) having a total collection angle of 2.02 sr.

Metal leaching was quantified using an Agilent 7900 ICP-MS equipped with an I-AS auto-sampler using a five-point calibration using certified reference materials from PerkinElmer and certified internal standard from Agilent. All calibrants were matrix-matched.

https://doi.org/10.1021/acscatal.2c03051
ACS Catal. 2022, 12, 11776–11789

RESULTS AND DISCUSSION

Our initial investigations established the efficacy of a range of Pd-based catalysts, synthesized via an excess chloride co-impregnation methodology,[28] toward the direct synthesis and subsequent degradation of H_2O_2 (Figure 1, with catalytic

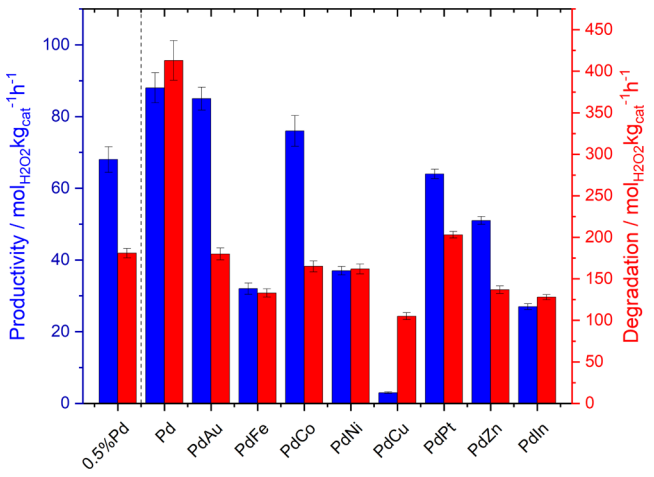

Figure 1. Catalytic activity of supported bimetallic catalysts toward the direct synthesis and degradation of H_2O_2, under high-pressure batch conditions. H_2O_2 direct synthesis reaction conditions: catalyst (0.01 g), H_2O (2.9 g), MeOH (5.6 g), 5% H_2/CO_2 (420 psi), 25% O_2/CO_2 (160 psi), 0.5 h, 2 °C, 1200 rpm. H_2O_2 degradation reaction conditions: catalyst (0.01 g), H_2O_2 (50 wt % 0.68 g) H_2O (2.22 g), MeOH (5.6 g), 5% H_2/CO_2 (420 psi), 0.5 h, 2 °C, 1200 rpm.

selectivity toward H_2O_2 and H_2 conversion rates reported in Table S3). These experiments were carried out under high-pressure batch reaction conditions, which have previously been optimized for H_2O_2 stability, namely, through the presence of an alcohol co-solvent and gaseous diluent (CO_2), which both contribute to the inhibition of H_2O_2 degradation pathways.[22] While these conditions are clearly not suitable for the chemo-enzymatic approach to cyclohexane oxidation, they are considered to allow for variation in catalytic performance toward H_2O_2 production to be better discerned.

In keeping with previous reports,[29−31] the alloying of Au with Pd was found to enhance catalytic efficiency, with selectivity toward H_2O_2 (54%) and rates of H_2O_2 degradation (180 $mol_{H_2O_2}$ kg_{cat}^{-1} h^{-1}), significantly improved compared to the analogous 1%Pd/TiO_2 catalyst (38% and 413 $mol_{H_2O_2}$ kg_{cat}^{-1} h^{-1}, respectively). However, this improvement in catalyst selectivity did not result in a concurrent increase in H_2O_2 synthesis rates, with the 0.5%Pd−0.5%Au/TiO_2 (85 $mol_{H_2O_2}$ kg_{cat}^{-1} h^{-1}) and 1%Pd/TiO_2 (88 $mol_{H_2O_2}$ kg_{cat}^{-1} h^{-1}) catalysts offering comparable activities. While this may not have been expected given the large number of studies into PdAu systems, which have typically reported a significant improvement in H_2O_2 synthesis upon formation of the alloy,[32] this observation aligns well with our previous studies into identically prepared catalysts and is attributed to the application of a reductive heat treatment during catalyst preparation, and the resulting formation of nanoparticles consisting of a random alloy composition.[33] Indeed, in many earlier studies, the use of an oxidative heat treatment, and the resulting formation of Au-core, Pd(oxide)-shell nanoparticle morphologies has been shown to be key in achieving enhanced selectivity toward H_2O_2.[34,35] It is noteworthy that while the activity of the 0.5%Pd−0.5%Au/TiO_2 catalyst toward H_2O_2 synthesis did not exceed that of the 1%Pd/TiO_2 catalyst, there was a considerable improvement compared to the 0.5%Pd/TiO_2 analogue (68 $mol_{H_2O_2}$ kg_{cat}^{-1} h^{-1}), which consists of an identical Pd loading. When considering the known limited activity of the Au component toward H_2O_2 production, it is, therefore, reasonable to conclude that there is indeed a synergistic enhancement from alloying the two metals.

The high catalytic performance of PdAu alloys toward H_2O_2 production has been extensively reported.[36,37] However, recent focus has shifted toward the introduction of a range of readily abundant metals into supported Pd nanoparticles,[38,39] this includes but is not limited to: Pb,[40] Co,[41] Cu,[42] Sn,[43] Ag,[44] Zn,[45] Ni,[46,47] In,[48] Fe[49] and Te.[50] Typically, the improved selectivity of the resulting bimetallic catalysts has been attributed to a combination of Pd oxidation state modification and a reduction of contiguous Pd ensembles, with extended domains of Pd^0 known to promote H_2O_2 degradation to H_2O.[30,36] In keeping with earlier studies, we also observe the enhanced catalytic efficacy that can be achieved through the alloying of Pd with a range of transition metals (Au, Fe, Co, Ni, Cu, Pt, Zn, In) (Figure 1), with a clear reduction in H_2O_2 degradation rate and a concurrent improvement in H_2O_2 selectivity also observed (Table S3). However, unlike with the PdAu formulation, the majority of these bimetallic catalysts were unable to achieve H_2O_2 synthesis rates greater than the 0.5%Pd/TiO_2 analogue, although the H_2O_2 synthesis activity of the 0.5%Pd−0.5%Co/TiO_2 catalyst (76 $mol_{H_2O_2}$ kg_{cat}^{-1} h^{-1}) is notable. Indeed, the incorporation of a number of secondary metals significantly reduced the H_2O_2 synthesis rate with the introduction of Cu in particular found to have a substantial deleterious effect on catalytic activity toward both the direct synthesis and subsequent degradation of H_2O_2. This is in keeping with previous experimental studies into precious-metal catalysts, which contain large quantities of Cu for the direct synthesis of H_2O_2[51] and theoretical investigations,[52] which have determined that the formation of the intermediate species is thermodynamically unfavorable over Cu-containing precious-metal surfaces. Although notably, we have recently reported the beneficial effect on catalytic performance toward H_2O_2 production achieved upon the introduction of low concentrations of Cu into PdAu nanoalloys.[42]

We next evaluated the catalytic activity of the supported 1% PdX/TiO_2 catalysts toward H_2O_2 production, under reaction conditions suitable for C−H bond activation when utilizing the chemo-enzymatic cascade system,[21] namely, at ambient temperature, low pressure (29 psi), and using a phosphate-buffered reaction medium (pH 6), with catalytic performance over a 2 h reaction time reported in Figure 2 (a comparison of catalytic activity toward H_2O_2 degradation, under identical reaction conditions, is reported in Figure S3, and associated supplementary note).

Unlike with our studies using a high-pressure batch system (Figure 1), differences in catalyst performance were found to be much reduced, with all catalysts synthesizing fairly comparable concentrations of H_2O_2, with the clear exception of the PdCu and PdPt catalysts. While the limited performance of the former material has been discussed, the seemingly low activity of the latter is noteworthy, particularly given the numerous studies into the application of PdPt catalysts for H_2O_2 synthesis and the relatively high rates of H_2O_2 synthesis observed under conditions optimized for H_2O_2 stability

https://doi.org/10.1021/acscatal.2c03051
ACS Catal. 2022, 12, 11776−11789

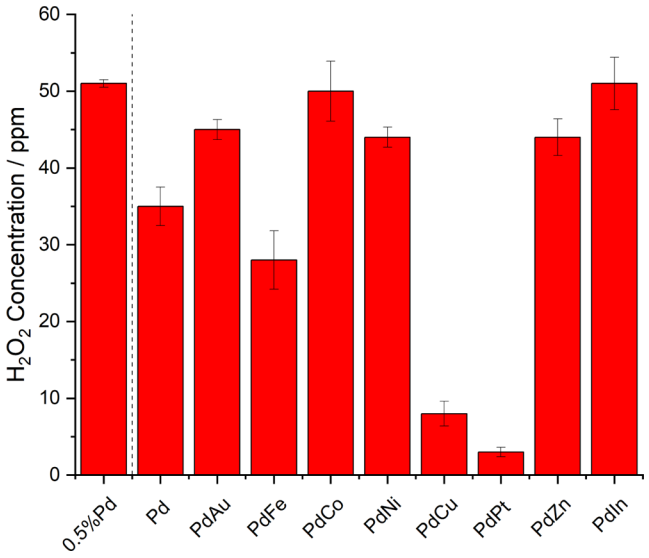

Figure 2. Catalytic activity of supported bimetallic catalysts toward the direct synthesis of H_2O_2, under low-pressure batch conditions. H_2O_2 direct synthesis reaction conditions: catalyst (0.001 g), phosphate buffer (100 mM, 10 mL, pH 6.0), using a gas mixture of 80% H_2/air H_2 (23 psi) and air (6 psi), 2 h, 20 °C, 250 rpm.

(Figure 1).[53,54] However, given the high partial pressures of H_2 used in this system, it is possible to attribute the limited H_2O_2 synthesis activity of the PdPt catalyst to the increased rates of H_2O_2 degradation, particularly through hydrogenation pathways.[55] Notably, under these reaction conditions, the 1%Pd/TiO_2 catalyst was found to synthesize somewhat less H_2O_2 (42 ppm) than many of the bimetallic catalysts and the 0.5%Pd/TiO_2 analogue (51 ppm), with this attributed in-part to the lower selectivity of this catalyst toward H_2O_2, as evidenced under conditions both optimized for H_2O_2 formation (Figure 1 and Table S3) and those utilized for the chemo-catalytic/enzymatic transformations (Figure S3).

With a focus on the 0.5%Pd−0.5%Au/TiO_2/PaDa-I system, we next established the significant improvement in cyclohexane oxidation activity achieved in the presence of H_2 and O_2, in comparison to that when either gaseous reagent (H_2 and O_2 (as air)) was used separately (Table S4). Indeed, the concentration of KA oil generated through in situ production of H_2O_2 was also found to be significantly greater than that observed when using preformed H_2O_2 both at elevated concentrations, identical to that if all of the H_2 in the system was converted to H_2O_2, or at concentrations comparable to that detected after a standard 2 h H_2O_2 direct synthesis experiment (50 ppm) (Table S4). It is noteworthy that in the case of this latter investigation, both commercially available H_2O_2 (i.e., in the presence of propriety stabilizers), and that generated in our high-pressure autoclave system, using an identical aqueous media to that used for the low-pressure studies and in the absence of stabilizers, was utilized. Interestingly, significantly higher rates of cyclohexane conversion were achieved via the in situ production of H_2O_2 (22.4%) compared to that obtained when using the preformed oxidant (~3.5%) at comparable concentrations, and this can be understood to be related in part to the complete addition of the oxidant at the start of the reaction and the susceptibility of the PaDa-I enzyme to high concentrations of H_2O_2.[14] Additionally, while the possible detrimental effects of the stabilizing agents present in commercial H_2O_2 on enzyme stability and the added complexity of product streams that would result from the use of the preformed oxidant should also be considered, particularly for application at scale, our studies do not suggest the presence of stabilizing agents has a detrimental effect, at least over the time scale studied.

Subsequently, we investigated the efficacy of the chemo-catalytic series, when used in conjunction with PaDa-I, for the selective oxidation of cyclohexane to the corresponding alcohol and ketone (KA oil) via in situ H_2O_2 production (Figure 3,

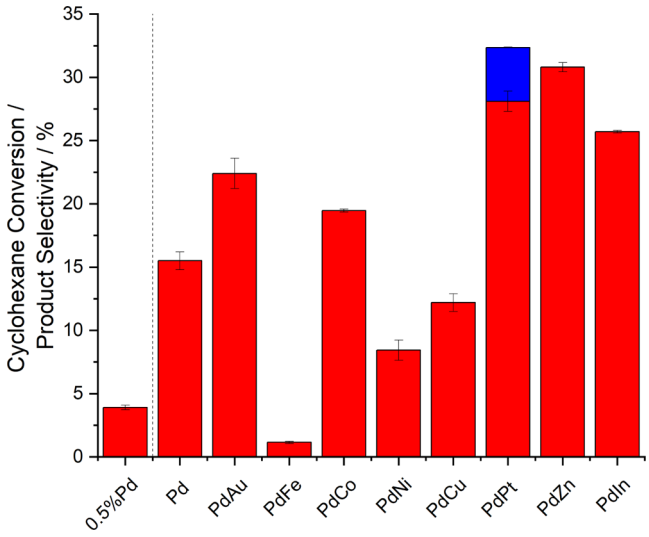

Figure 3. Catalytic activity of supported Pd-based catalysts toward the selective oxidation of cyclohexane in conjunction with PaDa-I. Key: cyclohexanol (red), cyclohexanone (blue). Cyclohexane oxidation reaction conditions: catalyst (0.001 g), cyclohexane (10 mM), PaDa-I (15 U mL_{RM}^{-1}), phosphate buffer (100 mM, 10 mL, pH 6.0), using a gas mixture of 80% H_2/air H_2 (23 psi) and air (6 psi), 2 h, 20 °C, 250 rpm.

with a comparison of reaction rates reported in Table S5). Perhaps expectedly given the observed synergy often reported through the alloying of Pd with Au[56] and the higher rates of H_2O_2 production observed over the bimetallic catalyst under identical reaction conditions (Figure 2), the 0.5%Pd−0.5%Au/TiO_2 catalyst was observed to offer higher activity toward cyclohexane oxidation (22.4% cyclohexane conversion) than the 1%Pd/TiO_2 analogue (15.5% cyclohexane conversion). Notably, the incorporation of Co (19.5% cyclohexane conversion), Pt (32.4% cyclohexane conversion), Zn (30.8% cyclohexane conversion), and In (25.7% cyclohexane conversion) was also found to improve cyclohexane conversion considerably compared to that observed over the monometallic Pd catalyst. Indeed, the latter three catalysts also outperformed the PdAu analogue, although a minor loss in selectivity toward cyclohexanol was observed over the 0.5%Pd−0.5%Pt/TiO_2 catalyst (86.7% cyclohexanol selectivity).

While the observed catalytic trends toward H_2O_2 production (Figure 2) may have led to the assumption that many of the chemo-catalysts studied would offer comparable activity toward cyclohexane oxidation, it is important to consider that in the presence of the PaDa-I enzyme any H_2O_2 generated by the heterogeneous catalyst will be readily utilized in the oxidation of cyclohexane, although the role of competitive chemo-catalytic-driven reactions, which result in the formation of H_2O, should also be considered. As such a comparison of initial reaction rates of H_2O_2 synthesis, where the contribution

https://doi.org/10.1021/acscatal.2c03051
ACS Catal. 2022, 12, 11776−11789

of H_2O_2 degradation pathways can be assumed to be negligible, may be considered a more accurate indication of the chemo-catalytic/enzymatic cascade system toward cyclohexane oxidation. Initial rates of H_2O_2 synthesis, in the absence of PaDa-I, are reported in Table 1, with catalytic performance toward H_2O_2 as a function of reaction time reported in Figure S4A,B.

Table 1. Comparison of H_2O_2 Direct Synthesis Reaction Rate over Supported PdX/TiO_2 Catalysts[a]

	rate of H_2O_2 synthesis ($mmol_{H_2O_2}/mmol_{metal}/h$)	
catalyst	5 min	120 min
0.5%Pd/TiO_2	3.05×10^2	1.61×10^2
1%Pd/TiO_2	1.91×10^2	5.54×10^1
0.5%Pd−0.5%Au/TiO_2	4.46×10^2	9.25×10^1
0.5%Pd−0.5%Fe/TiO_2	2.63×10^1	3.05×10^1
0.5%Pd−0.5%Co/TiO_2	2.99×10^2	5.64×10^1
0.5%Pd−0.5%Ni/TiO_2	1.90×10^2	4.95×10^1
0.5%Pd−0.5%Cu/TiO_2	1.14×10^2	9.47×10^0
0.5%Pd−0.5%Pt/TiO_2	2.47×10^2	6.15×10^0
0.5%Pd−0.5%Zn/TiO_2	3.48×10^2	5.3×10^0
0.5%Pd−0.5%In/TiO_2	3.56×10^2	8.38×10^1

[a]H_2O_2 direct synthesis reaction conditions: catalyst (0.001 g), phosphate buffer (100 mM, 10 mL, pH 6.0), using a gas mixture of 80% H_2/air (23 psi H_2, 6 psi air), 20 °C, 250 rpm.

While initial reaction rates toward H_2O_2 production can be seen to partially correlate with performance toward cyclohexane oxidation and certainly would identify the PdAu, PdZn, and PdIn formulations as choice candidates for use in the cascade reaction, the use of this metric alone to predict high efficacy toward the formation of KA oil is not entirely suitable, at least over the time frame studied. Indeed, based on initial H_2O_2 synthesis rates alone one would not expect the high cyclohexane conversion rates observed when utilizing the PdPt catalyst in conjunction with PaDa-I. These observed discrepancies are likely a result of variation in catalytic performance toward competitive H_2O_2 degradation reactions and in turn selectivity toward H_2O_2 over the course of the reaction. However, these investigations do possibly identify the need to balance the rate of H_2O_2 synthesis (over the chemo-catalyst) and its subsequent utilization (by the enzyme) to achieve optimal C−H bond activation.

With an aim to investigate the efficacy of the chemo-catalyst formulations, in conjunction with the PaDa-I enzyme, for the in situ cyclohexane oxidation, and with a concern around the role of leached metal species on the long-term performance and stability of the enzymatic component subsequent model studies determined the extent of leaching during the cyclohexane oxidation reaction (Table S6). Such studies were conducted at catalyst loadings (0.01 g) 10 times greater than that utilized for our low-pressure H_2O_2 direct synthesis studies, to allow for accurate determination of the extent of metal leaching. Notably, for all chemo-catalysts studied, the extent of Pd leaching is particularly low (<20 ppb in all cases). However, that of the secondary metals is typically greater than that observed for Pd and this is particularly so in the case of the PdCo and PdNi formulations.

With the potential loss of metal species via leaching processes identified under model reaction conditions (Table S6) and extrapolating to levels of homogeneous metal likely to be present under reaction conditions utilized for cyclohexane oxidation, we next set out to investigate the role of these species (as metal chlorides) on the efficiency of cyclohexane upgrading, when using preformed H_2O_2 (50 ppm) (Figure S5). For many of the metal species studied, the effect on overall performance was found to be negligible, with rates of cyclohexane conversion reached which were comparable to that observed when using PaDa-I alone. However, over a subset of the metals studied (Pd, Au, Pt, and In), cyclohexane conversion was somewhat reduced. While such observations may indicate the deleterious effect of homogeneous metals on the activity/stability of the enzyme, it is considered that this loss of performance results from the contribution of competitive H_2O_2 degradation, in particular given the reported activity of colloidal metals to promote such pathways.[57]

The selectivity of supported Pd-based catalysts toward H_2O_2 is known to depend on Pd oxidation state, with Pd^0 species typically more active toward undesirable competitive reaction pathways that lead to H_2O_2 degradation compared to Pd^{2+} analogous.[58−60] Although numerous studies have recently highlighted the enhanced efficacy of domains of mixed oxidation state (Pd^0−Pd^{2+}), compared to Pd^0- or Pd^{2+}-rich species.[61] Analysis of the Pd-based catalysts by XPS (Figure 4) indicates that Pd is present predominantly as Pd^0 in the case of the 1%Pd/TiO_2 catalyst. However, upon the introduction of all secondary metals, a significant shift, toward Pd^{2+} was observed, this is despite the application of a reductive heat treatment (5% H_2/Ar, 400 °C, 4 h) and clearly highlights the modification in Pd speciation that can be achieved through the formation of bimetallic alloys. It is therefore possible, at least in part, to correlate the enhanced activity of many of the bimetallic formulations with the formation of species consisting of mixed Pd oxidation states and an inhibition of competitive H_2O_2 degradation pathways (Figure 1), although it should be noted that the Pd speciation of the as-prepared materials is likely to not be fully representative of those present under reaction conditions.

With synergistic effects well known to result from the formation of PdAu alloys and the clear enhancement in performance as a result of the introduction of Zn into supported Pd nanoparticles, we were subsequently motivated to gain further insight into the underlying cause for the differences observed in catalytic reactivity and selectivity.

Extended reaction time studies comparing the efficacy of key catalysts toward cyclohexane oxidation can be seen in Figure 5. Given the total selectivity of the PdIn and PdCo formulations in addition to the relatively high rates of cyclohexane conversion, these formulations were also evaluated, with time-on-line data presented in Figure S6. As with standard reaction time (2 h) studies, the improved activity of the 0.5% Pd−0.5%Zn/TiO_2 catalyst is again clear, with rates of cyclohexane conversion (55.7%) far greater than that of either 0.5%Pd−0.5%Au/TiO_2 (42.0%) or 1%Pd/TiO_2 (30.5%) catalysts, over extended reaction times (8 h). It is noteworthy that while the formation of cyclohexanone was observed at extended reaction times over both the PdAu and PdZn catalysts, cyclohexanol selectivity was retained to a greater extent over the latter (93.7%) compared to the former (88.9%), despite the far higher rate of cyclohexane conversion observed over the PdZn formulation.

The high selectivity of the PdZn catalyst was further evidenced through a comparison of the catalytic series at iso-conversion (Figure 6). All three catalysts were observed to

https://doi.org/10.1021/acscatal.2c03051
ACS Catal. 2022, 12, 11776−11789

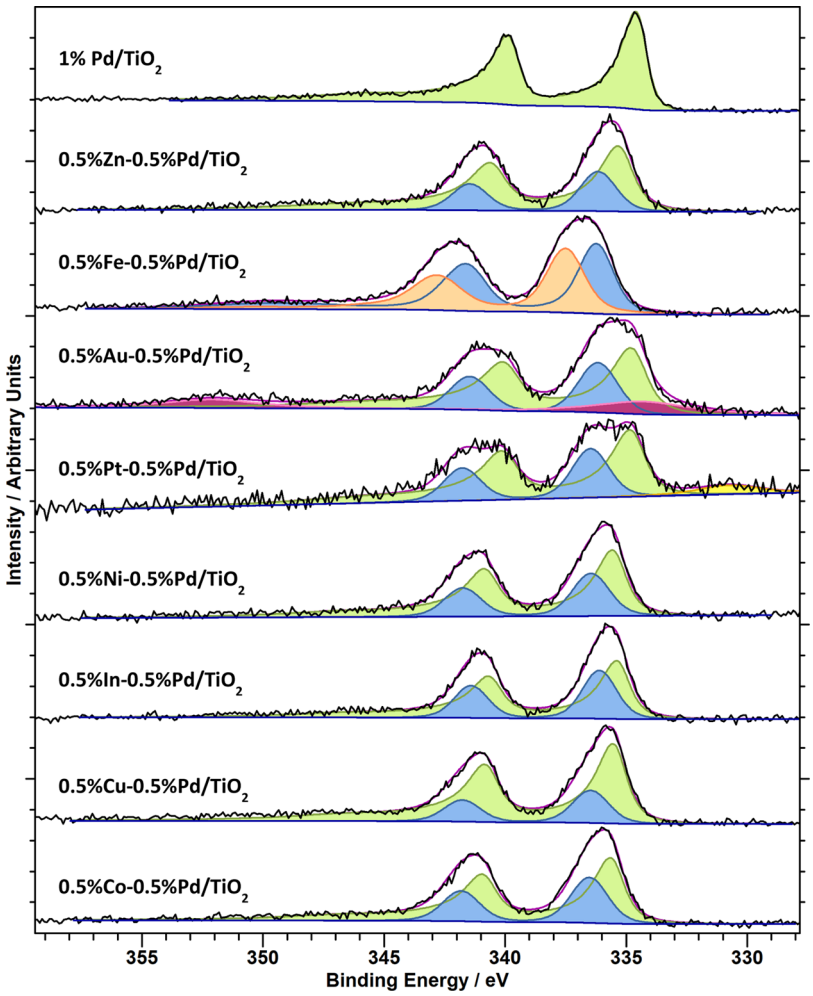

Figure 4. Surface atomic compositions of as-prepared Pd-based catalysts, prepared via an excess chloride co-impregnation procedure, as a function of secondary metal modifier, as determined by XPS using Pd (3d) regions. Key: Au^0 (pink), Pd^0 (green), Pd^{2+} i.e., PdO (blue), $PdCl_x$ (orange), Pt (yellow).

offer total selectivity toward cyclohexanol at relatively low rates of cyclohexane conversion ($\leq$ 30%). However, in keeping with our time-on-line study (Figure 5), the 0.5%Pd−0.5%Zn/TiO_2 catalyst was found to retain its total selectivity toward cyclohexanol at much higher rates of cyclohexane conversion (100% selectivity to cyclohexanol at 40% conversion), whereas some cyclohexanone was detected in the presence of the 0.5% Pd−0.5%Au/TiO_2 catalyst, at identical rates of substrate conversion (90% selectivity to cyclohexanol at 40% conversion). It should be noted that in the case of the 0.5%Pd−0.5%Zn/TiO_2 catalyst, this measure of catalytic performance was observed to decrease somewhat at even higher rates of conversion (94% selectivity to cyclohexanol at 55% conversion), although this metric was still higher than that observed over the PdAu analogue (90% selectivity to cyclohexanol at 55% conversion). Notably, the Pd-only catalyst was unable to attain such high rates of cyclohexane conversion to allow for comparison.

We subsequently set out to establish the contribution of this subset of catalysts toward the oxidation of cyclohexanol to the corresponding ketone (Figure S7), over a standard 2 h reaction time. Both an enzymatic and chemo-catalytic route to cyclohexanone formation were observed, although is clear that the former is the dominant pathway. Interestingly, it was found that the 0.5%Pd−0.5%Zn/TiO_2 catalyst alone was unable to catalyze the overoxidation of cyclohexanol over the timeframe investigated, whereas both the 1%Pd/TiO_2 and 0.5%Pd−0.5%Au/TiO_2 catalysts were indeed able to promote the formation of cyclohexanone. Although notably, the extent of overoxidation is far less than that observed over the PaDa-I enzyme, when supplied with a comparable concentration of preformed H_2O_2 to that synthesized by the heterogeneous catalysts (50 ppm). These observations are in keeping with our earlier findings, where the PdZn catalyst demonstrated improved selectivity to cyclohexanol compared to either the PdAu or Pd-only analogues (Figures 5 and 6).

Further investigation of the Pd-based catalysts via STEM-HAADF imaging revealed a considerable variation in mean nanoparticle size with catalyst composition. In keeping with previous studies,[53] the monometallic Pd catalyst was found to consist of small clusters in the sub-nano range with an absence of any larger (>3 nm) particles (Figure 7A,B). The alloying of Pd with Au resulted in the bifurcation of particle size, with a proportion of larger (5−20 nm) nanoparticles observed in addition to smaller clusters (Figure 7C). Subsequent STEM-XEDS mapping of individual nanoparticles, as presented in Figure 7D (additional analysis reported in Figures S8 and S9), confirmed that the larger particles consisted of random alloys of Pd and Au, while the smaller clusters were found to consist

https://doi.org/10.1021/acscatal.2c03051
ACS Catal. 2022, 12, 11776−11789

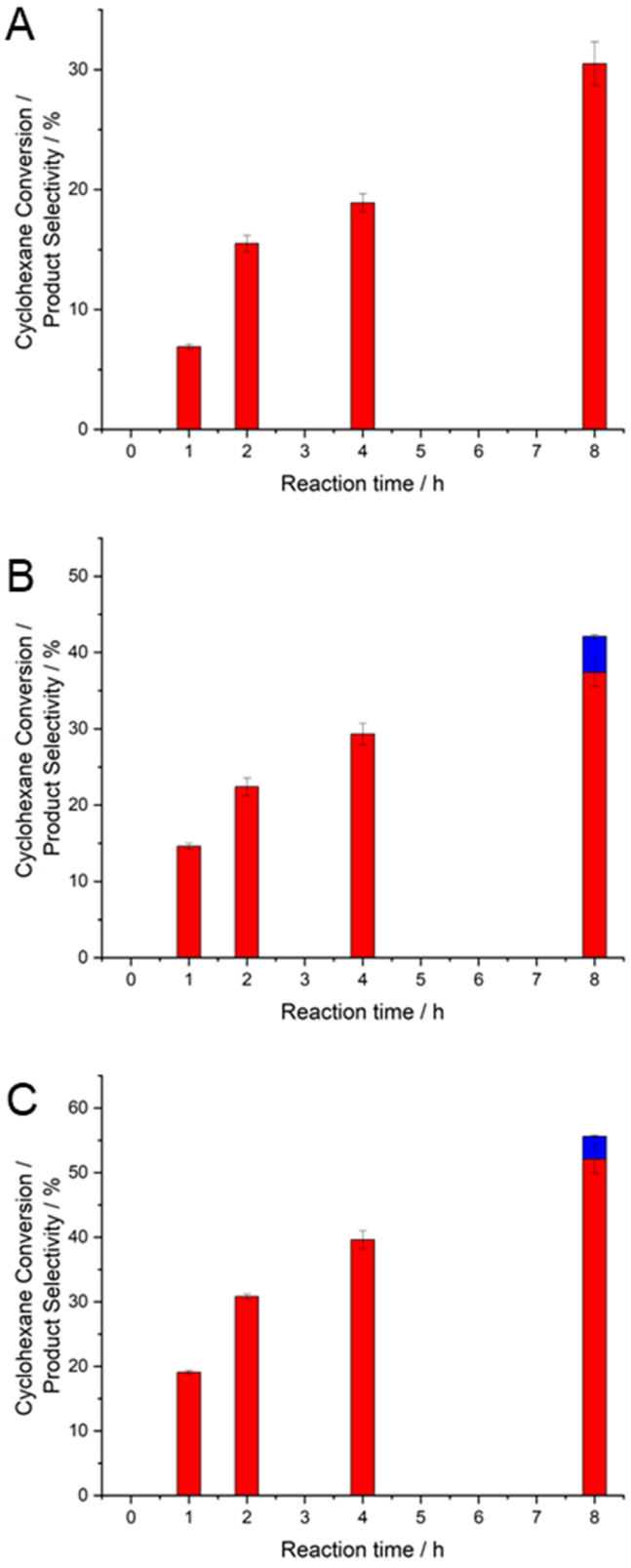

Figure 5. Comparison of the catalytic activity of (A) 1%Pd/TiO_2, (B) 0.5%Pd−0.5%Au/TiO_2, and (C) 0.5%Pd−0.5%Zn/TiO_2 when used in conjunction with PaDa-I toward the selective oxidation of cyclohexane, as a function of reaction time. Key: cyclohexanol (red), cyclohexanone (blue). Cyclohexane oxidation reaction conditions: catalyst (0.001 g), cyclohexane, PaDa-I (15 U mL_{RM}^{-1}), phosphate buffer (100 mM, 10 mL, pH 6.0), using a gas mixture of 80% H_2/air H_2 (23 psi) and air (6 psi), 20 °C, 250 rpm.

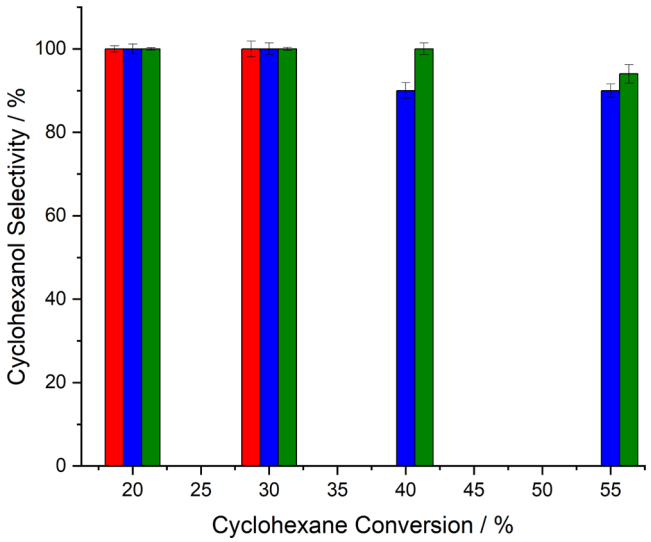

Figure 6. Comparison of catalytic selectivity of supported Pd-based catalysts when used in conjunction with PaDa-I, toward the selective oxidation of cyclohexane at iso-conversion. Key: 1%Pd/TiO_2 (red), 0.5%Pd−0.5%Au/TiO_2 (blue), 0.5%Pd−0.5%Zn/TiO_2 (green). Cyclohexane oxidation reaction conditions: catalyst (0.001 g), cyclohexane (10 mM), PaDa-I (15 U mL_{RM}^{-1}), phosphate buffer (100 mM, 10 mL, pH 6.0), 80% H_2/air (H_2 (23 psi) and air (6 psi)), 20 °C, 250 rpm. Note: the 1%Pd/TiO_2/PaDa-I system was unable to exceed 30% conversion.

of Pd only, which is again in keeping with our previous investigations into comparable materials.[9]

In a similar manner to the PdAu catalyst, the 0.5%Pd−0.5% Zn/TiO_2 analogue was also found to display a relatively wide particle size range, consisting of small clusters, nanoparticles (1−5 nm), and some larger agglomerates (Figure 8A,B). Although it should be noted that the agglomerates were few in number and well distributed over the support. XEDS elemental mapping revealed that the nanoparticles were alloys of Pd and Zn (Figure 8D). Additional evaluation of the clusters revealed a strong bimetallic interaction (Figure S10), contrary to that observed in the PdAu material. While it should be noted that such observations are not wholly definitive of the formation of bimetallic PdZn alloys, they are in keeping with investigations by Kozlov et al., and others who have shown that, unlike for PdAu materials, PdZn species readily alloy, with no significant dependency between particle size and elemental composition.[62,63]

With analysis by XPS revealing that the alloying of Pd with secondary metals results in a modification in Pd speciation (Figure 4), we subsequently probed the subset of key catalysts via CO-DRIFTS (Figure 9). Perhaps as expected, the DRIFTS spectra of the monometallic Pd and bimetallic PdAu and PdZn catalysts were dominated by Pd−CO bands. With a focus on the 1%Pd/TiO_2 catalyst, it is possible to attribute the peak observed at 2086 cm^{-1} to CO bonded to low-coordination Pd sites (i.e., corner and edge sites), while the peaks centered at 1944 and 1870 cm^{-1} represent the multifold adsorption of CO on extended Pd domains. The alloying of Pd with Au was found to result in a definite blueshift in the bands related to bridging CO species. Such a shift is in keeping with observations made by Wilson et al.[64] and can be attributed to the formation of PdAu alloys (as observed by our STEM-XEDS analysis) and in particular the segregation of Pd within the alloy structure corresponding to the occupation of lower

https://doi.org/10.1021/acscatal.2c03051
ACS Catal. 2022, 12, 11776−11789

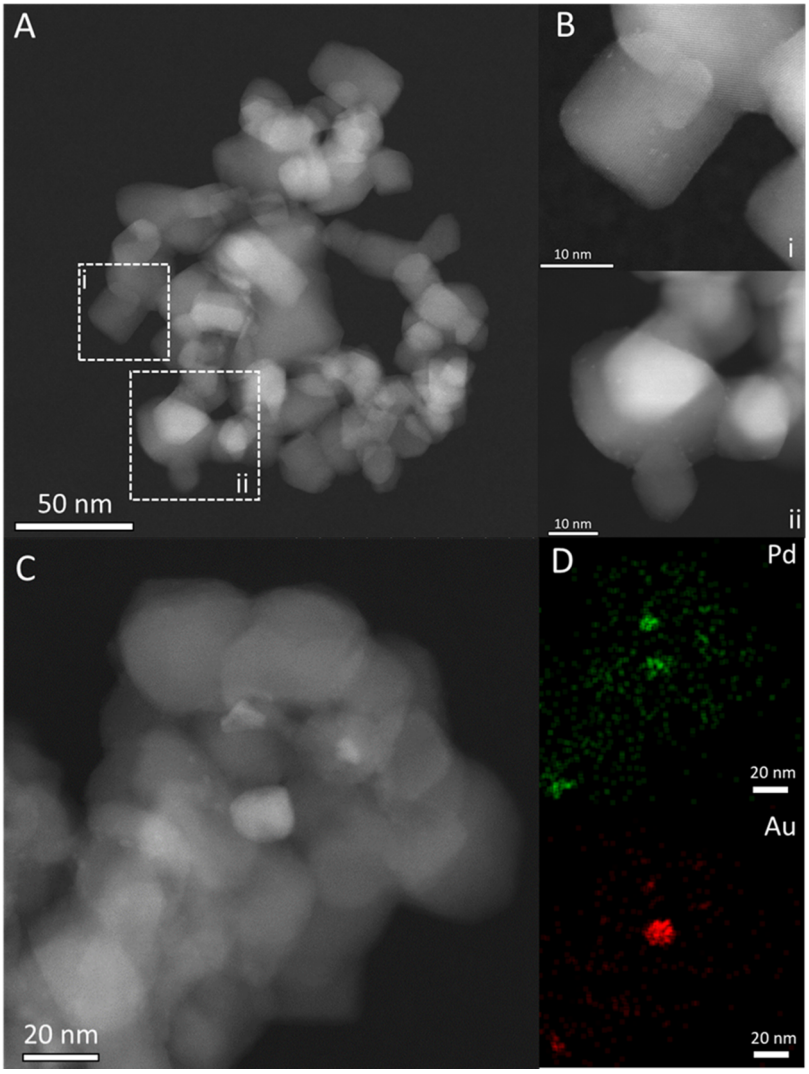

Figure 7. HAADF-STEM and X-EDS imaging of as-prepared Pd and PdAu catalyst. (A) Lower magnification of 1%Pd/TiO_2 showing the absence of larger particles, (B) high-magnification images of 1%Pd/TiO_2 from areas indicated showing small 1−2 nm Pd clusters on TiO_2 surface, (C) analysis of the 0.5%Pd−0.5%Au/TiO_2 catalyst showing both small (1−2 nm) and larger (5−20 nm) nanoparticles, and (D) Pd and Au XEDS maps of area in (C) showing the higher concentration of Pd in the smaller particles and alloying and Au-rich larger particles.

coordination sites. Upon the alloying of Pd with Zn, a similar blueshift was observed to that detected upon the introduction of Au, from 1870 cm^{-1} in the case of the 1%Pd/TiO_2 catalyst to 1880 cm^{-1} for the PdZn analogue. As previously reported by both Wang et al.[45] and Bahruji et al.[65] a near-total loss in the intensity of the band centered at 1944 cm^{-1} was detected upon formation of the PdZn alloy, with such observations characteristic of a substantial modification of Pd surface structures. Perhaps of more interest is the apparent blueshift observed in the band associated with CO bonded to low-coordination Pd sites upon Zn introduction. Such a shift can be considered to indicate the presence of a strong Pd−Zn interaction in the smaller metal clusters, in addition to the larger Pd domains, and is supportive of our prior STEM-XEDS analysis (Figure S10).

As such, we consider that the enhanced performance of the 0.5%Pd−0.5%Zn/TiO_2 catalyst in comparison to PdAu and Pd-only analogues can be related, at least in part, to a combination of enhanced PdZn interaction and subsequent electronic modification of Pd species.

CONCLUSIONS

We have demonstrated that through a tandem chemo-enzymatic process, it is possible to selectively oxidize cyclohexane to the corresponding alcohol and ketone (collectively known as KA oil), via in situ H_2O_2 production. This is achieved under reaction conditions where limited activity is observed using preformed H_2O_2 and represents an attractive alternative to current co-enzymatic systems or the continual introduction of preformed oxidant. The incorporation of Zn into Pd nanoparticles is seen to considerably improve catalytic activity compared to Pd-only or PdAu analogues, while also offering improved selectivity to cyclohexanol. The enhanced performance of the 0.5%Pd−0.5%Zn/TiO_2/PaDa-I system is attributed to the facile formation of PdZn alloys, with the significant population of Pd clusters present in both the PdAu and monometallic catalysts considered to be primarily responsible for promoting competitive side reactions. We consider that the materials developed within this study represent a promising basis for further investigation, for a range of chemical transformations which may utilize in situ generated H_2O_2, in particular given

https://doi.org/10.1021/acscatal.2c03051
ACS Catal. 2022, 12, 11776−11789

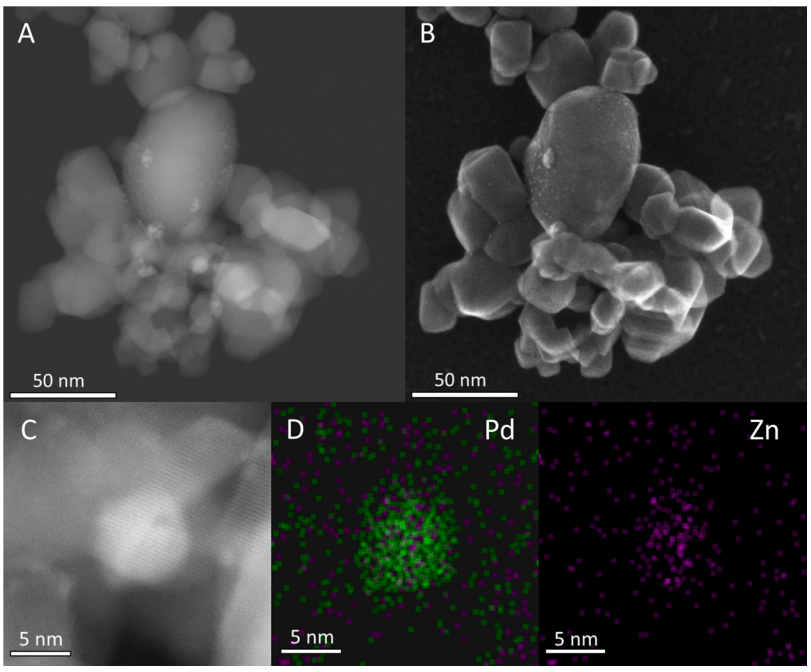

Figure 8. (A) HAADF-STEM and (B) secondary electron image of the 0.5%Pd−0.5%Zn/TiO_2 catalyst showing the presence of small clusters and larger particles. (C) HAADF-STEM and (D) X-EDS analyses of one of the larger particles showing alloying of the Pd and Zn.

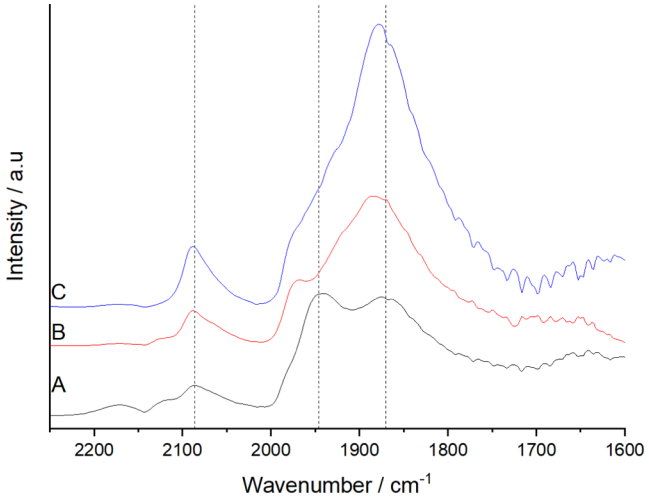

Figure 9. CO-DRIFTS spectra for (A) 1%Pd/TiO_2, (B) 0.5%Pd−0.5%Au/TiO_2, and (C) 0.5%Pd−0.5%Zn/TiO_2 catalysts.

the high selectivity to desirable products, which can be achieved through the alloying of Pd with earth-abundant metals.

■ ASSOCIATED CONTENT

Supporting Information

The Supporting Information is available free of charge at https://pubs.acs.org/doi/10.1021/acscatal.2c03051.

Data relating to chemo-catalytic testing for the direct synthesis of H_2O_2 and chemo-catalytic/enzymatic testing for the in situ oxidation of cyclohexane and cyclohexanol, with accompanying supplementary notes; data relating to the characterization of key materials via BET, XRD, HAADF-STEM, and X-EDS (PDF)

■ AUTHOR INFORMATION

Corresponding Authors

Richard J. Lewis − *Max Planck−Cardiff Centre on the Fundamentals of Heterogeneous Catalysis (FUNCAT), Cardiff Catalysis Institute, School of Chemistry, Cardiff University, Cardiff CF10 3AT, United Kingdom;* orcid.org/0000-0001-9990-7064; Email: LewisR27@Cardiff.ac.uk

Xi Liu − *In-situ Centre for Physical Sciences, School of Chemistry and Chemical, Frontiers Science Centre for Transformative Molecules, Shanghai 200240, P. R. China;* Email: LiuXi@edu.cn

Graham J. Hutchings − *Max Planck−Cardiff Centre on the Fundamentals of Heterogeneous Catalysis (FUNCAT), Cardiff Catalysis Institute, School of Chemistry, Cardiff University, Cardiff CF10 3AT, United Kingdom;* orcid.org/0000-0001-8885-1560; Email: Hutch@Cardiff.ac.uk

Authors

Joseph Brehm − *Max Planck−Cardiff Centre on the Fundamentals of Heterogeneous Catalysis (FUNCAT), Cardiff Catalysis Institute, School of Chemistry, Cardiff University, Cardiff CF10 3AT, United Kingdom*

Thomas Richards − *Max Planck−Cardiff Centre on the Fundamentals of Heterogeneous Catalysis (FUNCAT), Cardiff Catalysis Institute, School of Chemistry, Cardiff University, Cardiff CF10 3AT, United Kingdom*

Tian Qin − *In-situ Centre for Physical Sciences, School of Chemistry and Chemical, Frontiers Science Centre for Transformative Molecules, Shanghai 200240, P. R. China;* orcid.org/0000-0002-2856-4743

David J. Morgan − *Max Planck−Cardiff Centre on the Fundamentals of Heterogeneous Catalysis (FUNCAT), Cardiff Catalysis Institute, School of Chemistry, Cardiff University, Cardiff CF10 3AT, United Kingdom; HarwellXPS, Research Complex at Harwell (RCaH), Didcot*

https://doi.org/10.1021/acscatal.2c03051
ACS Catal. 2022, 12, 11776−11789

OX11 OFA, United Kingdom; orcid.org/0000-0002-6571-5731

Thomas E. Davies − *Max Planck−Cardiff Centre on the Fundamentals of Heterogeneous Catalysis (FUNCAT), Cardiff Catalysis Institute, School of Chemistry, Cardiff University, Cardiff CF10 3AT, United Kingdom*

Liwei Chen − *In-situ Centre for Physical Sciences, School of Chemistry and Chemical, Frontiers Science Centre for Transformative Molecules, Shanghai 200240, P. R. China; School of Chemistry and Chemical, Frontiers Science Centre for Transformative Molecules, Shanghai 200240, P. R. China;* orcid.org/0000-0003-4160-9771

Complete contact information is available at: https://pubs.acs.org/10.1021/acscatal.2c03051

Author Contributions

[⊥]J.B. and R.J.L. contributed equally to this work. J.B., R.J.L., and T.R. conducted catalyst synthesis, testing, and data analysis. J.B., R.J.L., T.R., T.Q., D.J.M., T.E.D., and X.L. conducted catalyst characterization and corresponding data processing. R.J.L., D.J.M., T.E.D., L.C., X.L., and G.J.H. provided technical advice and result interpretation. R.J.L. and G.J.H. conceived the design of the study. R.J.L. wrote the manuscript and the Supporting Information; all authors commented on and amended both documents. All authors discussed and contributed to the work.

Notes

The authors declare no competing financial interest.

■ ACKNOWLEDGMENTS

The authors gratefully acknowledge the Max Planck Centre for Fundamental Heterogeneous Catalysis (FUNCAT) for financial support. They thank the CCI-Electron Microscopy Facility which has been part-funded by the European Regional Development Fund through the Welsh Government and The Wolfson Foundation. X.L. thanks the National Key R&D Program of China (2021YFA1500300, 2021YFA1500303, 2021YFB3800300) and the National Natural Science Foundation of China (21991153, 21991150, 21872163, 22072090) for financial support. XPS data collection was performed at the EPSRC National Facility for XPS ("HarwellXPS"), operated by Cardiff University and UCL, under Contract No. PR16195.

■ REFERENCES

(1) Hu, B.-Y.; Yuan, Y.; Xiao, J.; Guo, C.; Liu, Q.; Tan, Z.; Li, Q. Rational oxidation of cyclohexane to cyclohexanol, cyclohexanone and adipic acid with air over metalloporphyrin and cobalt salt. *J. Porphyrins Phthalocyanines* **2008**, *12*, 27−34.

(2) Sun, L.; Liu, J.; Luo, W.; Yang, Y.; Wang, F.; Weerakkody, C.; Suib, S. L. Preparation of amorphous copper - chromium oxides catalysts for selective oxidation of cyclohexane. *Mol. Catal.* **2018**, *460*, 16−26.

(3) Wang, T.; She, Y.; Fu, H.; Li, H. Selective cyclohexane oxidation catalyzed by manganese porphyrins and co-catalysts. *Catal. Today* **2016**, *264*, 185−190.

(4) Hermans, I.; Jacobs, P. A.; Peeters, J. To the Core of Autocatalysis in Cyclohexane Autoxidation. *Chem. − Eur. J.* **2006**, *12*, 4229−4240.

(5) Khare, S.; Shrivastava, P. Solvent-free oxidation of cyclohexane over covalently anchored transition-metal salicylaldimine complexes to α-zirconium phosphate using tert-butylhydroperoxide. *J. Mol. Catal. A* **2016**, *411*, 279−289.

(6) Du, Y.; Xiong, Y.; Li, J.; Yang, X. Selective oxidation of cyclohexane with hydrogen peroxide in the presence of copper pyrophosphate. *J. Mol. Catal. A* **2009**, *298*, 12−16.

(7) Costa, A. A.; Ghesti, G. F.; de Macedo, J. L.; Braga, V. S.; Santos, M. M.; Dias, J. A.; Dias, S. C. L. Immobilization of Fe, Mn and Co tetraphenylporphyrin complexes in MCM-41 and their catalytic activity in cyclohexene oxidation reaction by hydrogen peroxide. *J. Mol. Catal. A* **2008**, *282*, 149−157.

(8) Crombie, C. M.; Lewis, R. J.; Kovačič, D.; Morgan, D. J.; Slater, T. J. A.; Davies, T. E.; Edwards, J. K.; Skjøth-Rasmussen, M. S.; Hutchings, G. J. The Selective Oxidation of Cyclohexane via In-situ H_2O_2 Production Over Supported Pd-based Catalysts. *Catal. Lett.* **2021**, *151*, 2762−2774.

(9) Crombie, C. M.; Lewis, R. J.; Kovačič, D.; Morgan, D. J.; Davies, T. E.; Edwards, J. K.; Skjøth-Rasmussen, M. S.; Hutchings, G. J. The Influence of Reaction Conditions on the Oxidation of Cyclohexane via the In-Situ Production of H_2O_2. *Catal. Lett.* **2021**, *151*, 164−171.

(10) Soussan, L.; Pen, N.; Belleville, M.-P.; Marcano, J. S.; Paolucci-Jeanjean, D. Alkane biohydroxylation: Interests, constraints and future developments. *J. Biotechnol.* **2016**, *222*, 117−142.

(11) Hofrichter, M.; Ullrich, R. Oxidations catalyzed by fungal peroxygenases. *Curr. Opin. Chem. Biol.* **2014**, *19*, 116−125.

(12) Wang, Y.; Lan, D.; Durrani, R.; Hollmann, F. Peroxygenases en route to becoming dream catalysts. What are the opportunities and challenges? *Curr. Opin. Chem. Biol.* **2017**, *37*, 1−9.

(13) Hrycay, E. G.; Bandiera, S. M. The monooxygenase, peroxidase, and peroxygenase properties of cytochrome P450. *Arch. Biochem. Biophys.* **2012**, *522*, 71−89.

(14) Ma, Y.; Li, Y.; Ali, S.; Li, P.; Zhang, W.; Rauch, M. C. R.; Willot, S. J.; Ribitsch, D.; Choi, Y. H.; Alcalde, M.; Hollmann, F.; Wang, Y. Natural Deep Eutectic Solvents as Performance Additives for Peroxygenase Catalysis. *ChemCatChem* **2020**, *12*, 989−994.

(15) Ma, Y.; Li, P.; Li, Y.; Willot, S. J.; Zhang, W.; Ribitsch, D.; Choi, Y. H.; Verpoorte, R.; Zhang, T.; Hollmann, F.; Wang, Y. Natural Deep Eutectic Solvents as Multifunctional Media for the Valorization of Agricultural Wastes. *ChemSusChem* **2019**, *12*, 1310−1315.

(16) Smeets, V.; Baaziz, W.; Ersen, O.; Gaigneaux, E. M.; Boissière, C.; Sanchez, C.; Debecker, D. P. Hollow zeolite microspheres as a nest for enzymes: a new route to hybrid heterogeneous catalysts. *Chem. Sci.* **2020**, *11*, 954−961.

(17) Vennestrøm, P. N. R.; Taarning, E.; Christensen, C. H.; Pedersen, S.; Grunwaldt, J.; Woodley, J. M. Chemoenzymatic Combination of Glucose Oxidase with Titanium Silicate-1. *ChemCatChem* **2010**, *2*, 943−945.

(18) Tieves, F.; Willot, S. J.; van Schie, M. M. C. H.; Rauch, M. C. R.; Younes, S. H. H.; Zhang, W.; Dong, J.; Gomez de Santos, P.; Robbins, J. M.; Bommarius, B.; Alcalde, M.; Bommarius, A. S.; Hollmann, F. Formate Oxidase (FOx) from Aspergillus oryzae: One Catalyst Enables Diverse H_2O_2-Dependent Biocatalytic Oxidation Reactions. *Angew. Chem., Int. Ed.* **2019**, *58*, 7873−7877.

(19) Perez, D. I.; Grau, M. M.; Arends, I. W. C. E.; Hollmann, F. Visible light-driven and chloroperoxidase-catalyzed oxygenation reactions. *Chem. Commun.* **2009**, 6848−6850.

(20) Wilson, N. M.; Priyadarshini, P.; Kunz, S.; Flaherty, D. W. Direct synthesis of H_2O_2 on Pd and Au_xPd_1 clusters: Understanding the effects of alloying Pd with Au. *J. Catal.* **2018**, *357*, 163.

(21) Freakley, S. J.; Kochius, S.; van Marwijk, J.; Fenner, C.; Lewis, R. J.; Baldenius, K.; Marais, S. S.; Opperman, D. J.; Harrison, S. T. L.; Alcalde, M.; Smit, M. S.; Hutchings, G. J. A chemo-enzymatic oxidation cascade to activate C−H bonds with in situ generated H_2O_2. *Nat. Commun.* **2019**, *10*, No. 4178.

(22) Santos, A.; Lewis, R. J.; Malta, G.; Howe, A. G. R.; Morgan, D. J.; Hampton, E.; Gaskin, P.; Hutchings, G. J. Direct Synthesis of Hydrogen Peroxide over Au−Pd Supported Nanoparticles under Ambient Conditions. *Ind. Eng. Chem. Res.* **2019**, *58*, 12623−12631.

(23) Jeon, J.; Kim, S. J. Recent Progress in Hydrogen Flammability Prediction for the Safe Energy Systems. *Energies* **2020**, *13*, 6263.

(24) Wang, Y.; Zhang, N.; Hübner, R.; Tan, D.; Löffler, M.; Facsko, S.; Zhang, E.; Ge, Y.; Qi, Z.; Wu, C. Enzymes Immobilized on Carbon

Nitride (C_3N_4) Cooperating with Metal Nanoparticles for Cascade Catalysis. *Adv. Mater. Interfaces* **2019**, *6*, No. 1801664.
(25) Brindle, J. S.; Nelson, P. S.; Charde, R. P.; Sufyan, S. A.; Nigra, M. M. Catalytically cooperativity between glucose oxidase and gold nanoparticles in the sequential oxidation of glucose to saccharic acid. *Green Chem.* **2022**, *24*, 5162−5170.
(26) Molina-Espeja, P.; Garcia-Ruiz, E.; Gonzalez-Perez, D.; Ullrich, R.; Hofrichter, M.; Alcalde, M. Directed Evolution of Unspecific Peroxygenase from *Agrocybe aegerita*. *Appl. Environ. Microbiol.* **2014**, *80*, 3496−3507.
(27) Scofield, J. H. Hartree-Slater subshell photoionization cross-sections at 1254 and 1487 eV. *J. Electron Spectrosc. Relat. Phenom.* **1976**, *8*, 129−137.
(28) Brehm, J.; Lewis, R. J.; Morgan, D. J.; Davies, T. E.; Hutchings, G. J. The Direct Synthesis of Hydrogen Peroxide over AuPd Nanoparticles: An Investigation into Metal Loading. *Catal. Lett.* **2022**, *152*, 254−262.
(29) Richards, T.; Harrhy, J. H.; Lewis, R. J.; Howe, A. G. R.; Suldecki, G. M.; Folli, A.; Morgan, D. J.; Davies, T. E.; Loveridge, E. J.; Crole, D. A.; Edwards, J. K.; Gaskin, P.; Kiely, C. J.; He, Q.; Murphy, D. M.; Maillard, J.; Freakley, S. J.; Hutchings, G. J. A residue-free approach to water disinfection using catalytic in situ generation of reactive oxygen species. *Nat. Catal.* **2021**, *4*, 575−585.
(30) Flaherty, D. W. Direct synthesis of H_2O_2 from H_2 and O_2 on Pd Catalysts: Current Understanding, Outstanding Questions, and Research needs. *ACS Catal.* **2018**, *8*, 1520−1527.
(31) Zhang, Y.; Lyu, Z.; Chen, Z.; Zhu, S.; Shi, Y.; Chen, R.; Xie, M.; Yao, Y.; Chi, M.; Shao, M.; Xia, Y. Maximizing the Catalytic Performance of Pd@Au_xPd_{1-x} Nanocubes in H_2O_2 Production by Reducing Shell Thickness to Increase Compositional Stability. *Angew. Chem., Int. Ed.* **2021**, *60*, 19643−19647.
(32) Beletskaya, A. V.; Pichugina, D. A.; Shestakov, A. F.; Kuz'menko, N. E. Formation of H_2O_2 on Au_{20} and $Au_{19}Pd$ Clusters: Understanding the Structure Effects on the Atomic Level. *J. Phys. Chem. A* **2013**, *117*, 6817.
(33) Richards, T.; Lewis, R. J.; Morgan, D. J.; Hutchings, G. J. The Direct Synthesis of Hydrogen Peroxide Over Supported Pd-Based Catalysts: An Investigation into the Role of the Support and Secondary Metal Modifiers. *Catal. Lett.* **2022**, DOI: 10.1007/s10562-022-03967-8.
(34) Cybula, A.; Priebe, J. B.; Pohl, M.-M.; Sobczak, J. W.; Schneider, M.; Zielińska-Jurek, A.; Brückner, A.; Zaleska, A. The effect of calcination temperature on structure and photocatalytic properties of Au/Pd nanoparticles supported on TiO_2. *Appl. Catal., B* **2014**, *152*−*153*, 202−211.
(35) Edwards, J. K.; Thomas, A.; Carley, A. F.; Herzing, A. A.; Kiely, C. J.; Hutchings, G. J. Au−Pd supported nanocrystals as catalysts for the direct synthesis of hydrogen peroxide from H_2 and O_2. *Green Chem.* **2008**, *10*, 388−394.
(36) Li, J.; Ishihara, T.; Yoshizawa, K. Theoretical Revisit of the Direct Synthesis of H_2O_2 on Pd and Au@Pd Surfaces: A Comprehensive Mechanistic Study. *J. Phys. Chem. C* **2011**, *115*, 25359−25367.
(37) Nomura, Y.; Ishihara, T.; Hata, Y.; Kitawaki, K.; Kaneko, K.; Matsumoto, H. Nanocolloidal Pd-Au as Catalyst for the Direct Synthesis of Hydrogen Peroxide from H_2 and O_2. *ChemSusChem* **2008**, *1*, 619−621.
(38) Wang, Y.; Pan, H.; Lin, Q.; Shi, Y.; Zhang, J. Synthesis of Pd-M@HCS(M = Co, Ni, Cu) Bimetallic Catalysts and Their Catalytic Performance for Direct Synthesis of H_2O_2. *Catalysts* **2020**, *10*, 303.
(39) Xu, H.; Cheng, D.; Gao, Y. Design of High-Performance Pd-Based Alloy Nanocatalysts for Direct Synthesis of H_2O_2. *ACS Catal.* **2017**, *7*, 2164−2170.
(40) Cao, K.; Yang, H.; Bai, S.; Xu, Y.; Yang, C.; Wu, Y.; Xie, M.; Cheng, T.; Shao, Q.; Huang, X. Efficient Direct H_2O_2 Synthesis Enabled by PdPb Nanorings via Inhibiting the O−O Bond Cleavage in O_2 and H_2O_2. *ACS Catal.* **2021**, *11*, 1106−1118.
(41) Nazeri, H.; Najafi Chermahini, A.; Mohammadbagheri, Z.; Prato, M. Direct production of hydrogen peroxide over bimetallic CoPd catalysts: Investigation of the effect of Co addition and calcination temperature. *Green Energy Environ.* **2021**, DOI: 10.1016/j.gee.2021.03.014.
(42) Barnes, A.; Lewis, R. J.; Morgan, D. J.; Davies, T. E.; Hutchings, G. J. Enhancing catalytic performance of AuPd catalysts towards the direct synthesis of H_2O_2 through incorporation of base metals. *Catal. Sci. Technol.* **2022**, *12*, 1986−1995.
(43) Freakley, S. J.; He, Q.; Harrhy, J. H.; Lu, L.; Crole, D. A.; Morgan, D. J.; Ntainjua, E. N.; Edwards, J. K.; Carley, A. F.; Borisevich, A. Y.; Kiely, C. J.; Hutchings, G. J. Palladium-tin catalysts for the direct synthesis of H_2O_2 with high selectivity. *Science* **2016**, *351*, 965−968.
(44) Zhang, J.; Huang, B.; Shao, Q.; Huang, X. Highly Active, Selective and Stable Direct H_2O_2 Generation by Monodispersive Pd-Ag Nanoalloy. *ACS Appl. Mater. Interfaces* **2018**, *10*, 21291−21296.
(45) Wang, S.; Gao, K.; Li, W.; Zhang, J. Effect of Zn addition on the direct synthesis of hydrogen peroxide over supported palladium catalysts. *Appl. Catal., A* **2017**, *531*, 89−95.
(46) Crole, D. A.; Underhill, R.; Edwards, J. K.; Shaw, G.; Freakley, S. J.; Hutchings, G. J.; Lewis, R. J. The direct synthesis of hydrogen peroxide from H_2 and O_2 using PdNi/TiO_2 catalysts. *Philos. Trans. R. Soc. A* **2020**, *378*, No. 20200062.
(47) Huynh, T.-T.; Huang, W.; Tsai, M.; Nugraha, M.; Haw, S.; Lee, J.; Su, W.; Hwang, B. J. Synergistic Hybrid Support Comprising TiO_2−Carbon and Ordered PdNi Alloy for Direct Hydrogen Peroxide Synthesis. *ACS Catal.* **2021**, *11*, 8407−8416.
(48) Wang, S.; Lewis, R.; Doronkin, D. E.; Morgan, D.; Grunwaldt, J.-D.; Hutchings, G.; Behrens, S. The Direct Synthesis of Hydrogen Peroxide from H_2 and O_2 Using Pd-Ga and Pd-In Catalysts. *Catal. Sci. Technol.* **2020**, *10*, 1925−1932.
(49) Santos, A.; Lewis, R. J.; Morgan, D. J.; Davies, T. E.; Hampton, E.; Gaskin, P.; Hutchings, G. J. The degradation of phenol via in situ H_2O_2 production over supported Pd-based catalysts. *Catal. Sci. Technol.* **2021**, *11*, 7866−7874.
(50) Tian, P.; Xuan, F.; Ding, D.; Sun, Y.; Xu, X.; Li, W.; Si, R.; Xu, J.; Han, Y. Revealing the role of tellurium in palladium-tellurium catalysts for the direct synthesis of hydrogen peroxide. *J. Catal.* **2020**, *385*, 21−29.
(51) Alotaibi, F.; Al-Mayman, S.; Alotaibi, M.; Edwards, J. K.; Lewis, R. J.; Alotaibi, R.; Hutchings, G. J. Direct Synthesis of Hydrogen Peroxide Using Cs-Containing Heteropolyacid-Supported Palladium−Copper Catalysts. *Catal. Lett.* **2019**, *149*, 998−1006.
(52) Joshi, A. M.; Delgass, W. N.; Thomson, K. T. Investigation of Gold−Silver, Gold−Copper, and Gold−Palladium Dimers and Trimers for Hydrogen Peroxide Formation from H_2 and O_2. *J. Phys. Chem. A* **2007**, *111*, 7384−7395.
(53) Han, G.-H.; Xiao, X.; Hong, J.; Lee, K.; Park, S.; Ahn, J.-P.; Lee, K.; Yu, T. Tailored Palladium−Platinum Nanoconcave Cubes as High Performance Catalysts for the Direct Synthesis of Hydrogen Peroxide. *ACS Appl. Mater. Interfaces* **2020**, *12*, 6328−6335.
(54) Sterchele, S.; Biasi, P.; Centomo, P.; Canton, P.; Campestrini, S.; Salmi, T.; Zecca, M. Pd-Au and Pd-Pt catalysts for the direct synthesis of hydrogen peroxide in absence of selectivity enhancers. *Appl. Catal., A* **2013**, *468*, 160−174.
(55) Gong, X.; Lewis, R. J.; Zhou, S.; Morgan, D. J.; Davies, T. E.; Liu, X.; Kiely, C. J.; Zong, B.; Hutchings, G. J. Enhanced catalyst selectivity in the direct synthesis of H_2O_2 through Pt incorporation into TiO_2 supported AuPd catalysts. *Catal. Sci. Technol.* **2020**, *10*, 4635−4644.
(56) Lewis, R. J.; Hutchings, G. J. Recent Advances in the Direct Synthesis of H_2O_2. *ChemCatChem* **2019**, *11*, 298−308.
(57) Freakley, S. J.; Agarwal, N.; McVicker, R. U.; Althahban, S.; Lewis, R. J.; Morgan, D. J.; Dimitratos, N.; Kiely, C. J.; Hutchings, G. J. Gold-palladium colloids as catalysts for hydrogen peroxide synthesis, degradation and methane oxidation: effect of the PVP stabiliser. *Catal. Sci. Technol.* **2020**, *10*, 5935−5944.
(58) Choudhary, V. R.; Gaikwad, A. G.; Sansare, S. D. Activation of supported Pd metal catalysts for selective oxidation of hydrogen to hydrogen peroxide. *Catal. Lett.* **2002**, *83*, 235−239.

(59) Gaikwad, A. G.; Sansare, S. D.; Choudhary, V. R. Direct oxidation of hydrogen to hydrogen peroxide over Pd-containing fluorinated or sulfated Al_2O_3, ZrO_2, CeO_2, ThO_2, Y_2O_3 and Ga_2O_3 catalysts in stirred slurry reactor at ambient conditions. *J. Mol. Catal. A* **2002**, *181*, 143−149.
(60) Blanco-Brieva, G.; Cano-Serrano, E.; Campos-Martin, J. M.; Fierro, J. L. G. Direct synthesis of hydrogen peroxide solution with palladium-loaded sulfonic acid polystyrene resins. *Chem. Commun.* **2004**, 1184−1185.
(61) Ouyang, L.; Tian, P.; Da, G.; Xu, X.; Ao, C.; Chen, T.; Si, R.; Xu, J.; Han, Y. The origin of active sites for direct synthesis of H_2O_2 on Pd/TiO_2 catalysts: Interfaces of Pd and PdO domains. *J. Catal.* **2015**, *321*, 70−80.
(62) Bowker, M.; Lawes, N.; Gow, I.; Hayward, J.; Esquius, J. R.; Richards, N.; Smith, L. R.; Slater, T. J. A.; Davies, T. E.; Dummer, N. F.; Kabalan, L.; Logsdail, A.; Catlow, R. C.; Taylor, S.; Hutchings, G. J. The Critical Role of βPdZn Alloy in Pd/ZnO Catalysts for the Hydrogenation of Carbon Dioxide to Methanol. *ACS Catal.* **2022**, *12*, 5371−5379.
(63) Kozlov, S. M.; Kovacs, F. R.; Ferrando, R.; Neyman, K. M. How to determine accurate chemical ordering in several nanometer large bimetallic crystallites from electronic structure calculations. *Chem. Sci.* **2015**, *6*, 3868−3880.
(64) Wilson, A. R.; Sun, K.; Chi, M.; White, R. M.; LeBeau, J. M.; Lamb, H. H.; Wiley, B. J. From Core−Shell to Alloys: The Preparation and Characterization of Solution-Synthesized AuPd Nanoparticle Catalysts. *J. Phys. Chem. A* **2013**, *117*, 17557−17566.
(65) Bahruji, H.; Esquius, J. R.; Bowker, M.; Hutchings, G.; Armstrong, R. D.; Jones, W. Solvent Free Synthesis of $PdZn/TiO_2$ Catalysts for the Hydrogenation of CO_2 to Methanol. *Top. Catal.* **2018**, *61*, 144−153.

https://doi.org/10.1021/acscatal.2c03051
ACS Catal. 2022, 12, 11776−11789